The Astrophysical Journal, 949:122 (4pp), 2023 June 1 https://doi.org/10.3847/1538-4357/acd453
© 2023. The Author(s). Published by the American Astronomical Society.
OPEN ACCESS

Erratum: "Molecular Outflows in $z > 6$ Unobscured QSO Hosts Driven by Star Formation" (2023, ApJ, 944, 134)

Kirsty M. Butler[1,2], Paul P. van der Werf[2], Theodoros Topkaras[2], Matus Rybak[2,3], Bram P. Venemans[2], Fabian Walter[4], and Roberto Decarli[5]
[1] Institut de Radioastronomie Millimétrique (IRAM), 300 rue de la Piscine, F-38400 Saint-Martin-d'Héres, France; kirstymaybutler@gmail.com
[2] Leiden Observatory, Leiden University, PO Box 9513, 2300 RA Leiden, The Netherlands
[3] THz Sensing Group, Faculty of Electrical Engineering, Mathematics and Computer Science, TU Delft, The Netherlands
[4] Max-Planck Institute for Astronomy, Konigstuhl 17, D-69117 Heidelberg, Germany
[5] INAF—Osservatorio di Astrofisica e Scienza dello Spazio di Bologna, via Gobetti 93/3, I-40129, Bologna, Italy
Received 2023 May 2; published 2023 June 5

1. Equivalent Width and Derived Properties

In this erratum, we correct a mistake in the derivation of OH 119 μm equivalent width in two sources: J2310+1855 and P183+05. Consequently, we also correct the molecular gas outflow mass, mass outflow rate (MOFR), momentum flux, kinetic energy flux, and depletion times as the derivation of these values involves the equivalent width. We provide an updated version of Table 3 from the published article, and of Figures 3, 5, and 6.

We no longer find significantly larger OH 119 μm absorption EWs in our unobscured QSO sources with respect to the high-z DSFGs from the literature Spilker et al. (2020a, 2020b).

Furthermore, the MOFR, momentum flux, and kinetic energy of the molecular outflows in J2310+1855 and P183+05, as traced by the blueshifted OH 119 μm absorption, are now all significantly offset to lower values with respect to the trends with far-infrared (FIR) luminosity seen in high-z DSFGs (Spilker et al. 2020a, 2020b). Even with an assumed 50% contribution to the FIR luminosity from the central active nucleus, both galaxies appear to have suppressed outflow properties. The star formation rate (SFR) exceeds the MOFR in both sources and is therefore the dominant mechanism responsible for depleting the molecular gas reservoir in these systems. The original conclusion of the published article is therefore unchanged and even reinforced.

We would like to thank Tom Bakx for bringing this error to our attention.

Original content from this work may be used under the terms of the Creative Commons Attribution 4.0 licence. Any further distribution of this work must maintain attribution to the author(s) and the title of the work, journal citation and DOI.

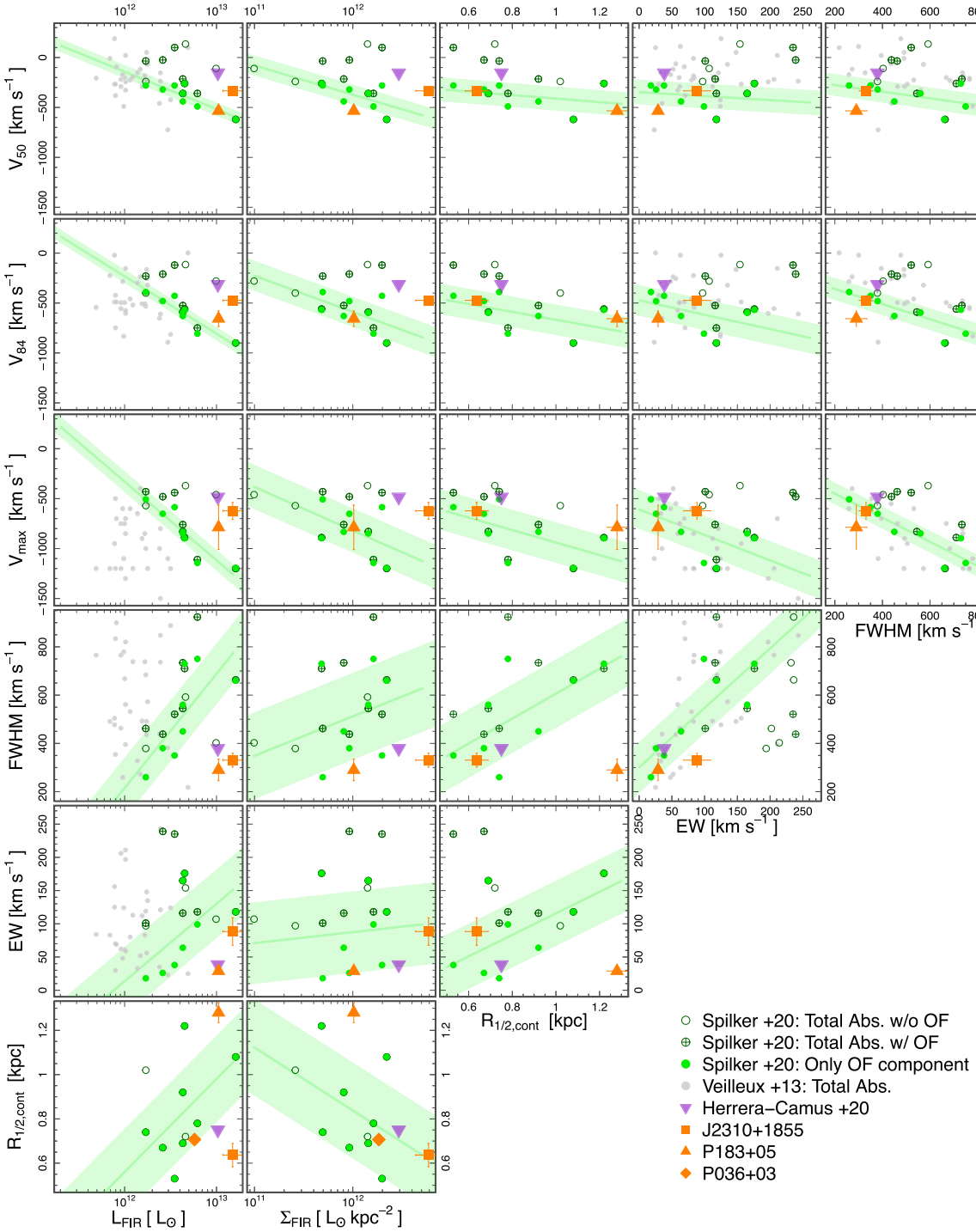

Figure 3. Grid of host galaxy and best-fit OH 119 μm absorption spectra properties. This includes: v_{50}: mean velocity, v_{84}: velocity above which 84% of the absorption lies, $v_{\rm max}$: velocity above which 98% of the absorption lies, FWHM of the absorption, EW: equivalent width of the absorption, $L_{\rm FIR}$: FIR luminosity of the host galaxy, $\Sigma_{\rm FIR}$: FIR surface brightness of the host galaxy given by $L_{\rm FIR}/(2\pi R_{1/2,\rm cont}^2)$, $R_{\rm cont}$: effective radius of the 119 μm continuum emission. We show low-z sources in gray, including both star-forming and active galactic nucleus (AGN) host galaxies (Veilleux et al. 2013). The spectral properties are measurements of the total (systemic and blueshifted) absorption lines. In green we show the high-z DSFG sample studied by Spilker et al. (2020a, 2020b), further separating this sample into measurements of the total (systemic and blueshifted) absorption line (dark green crossed circles), just the systemic components (dark green open circles), and just the outflowing components (light green filled). Sources with only an outflowing component will appear as a light green dot with a dark green outline. We display a fit to the outflow—only components in each panel (illustrative only) with a solid line and shade the 1σ scatter, both in light green. We include the tentative OH detection in the $z = 6.13$ QSO, ULAS J131911+095051 (Herrera-Camus et al. 2020; purple triangle). J2310+1855 and P183+05 are shown by the filled orange square and triangle, respectively.

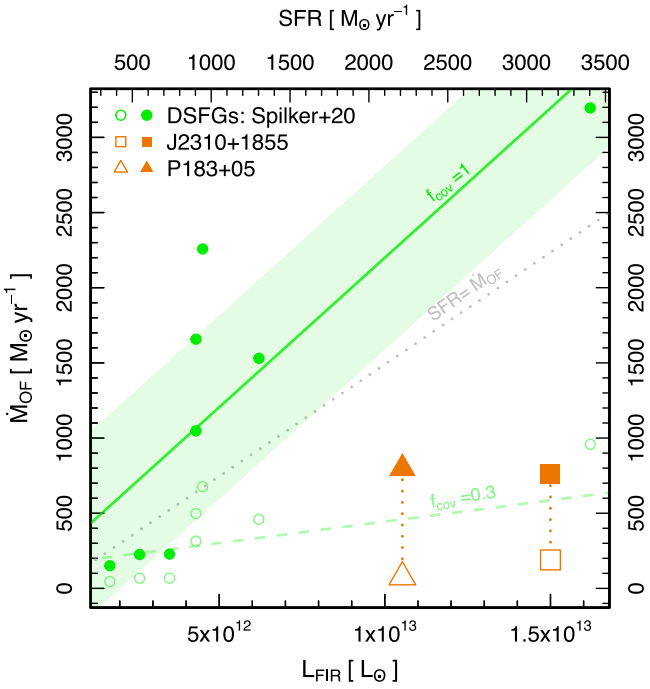

Figure 5. Mass outflow rate as a function of FIR luminosity (bottom axis) and star formation rate (top axis), assuming a spherical thin shell geometry for all sources. We show the DSFGs (Spilker et al. 2020a, 2020b) in green assuming a covering fraction of 1 (filled) as upper limits and 0.3 (hollow) based on the average covering fractions measured for low-z star-forming galaxies (González-Alfonso et al. 2017). We show a fit to the $f_{\rm cov} = 1$ points with the solid green line and its 1σ spread with a shaded green region. A fit to the $f_{\rm cov} = 0.3$ points is shown by the dashed green line. We indicate J2310+1855 and P183+05 with an orange square and triangle, assuming a covering fraction of 1 (filled) as upper limits and at the level of their fractional OH absorption depths, 25% and 9.4% (hollow), respectively. The SFR $= \dot{M}_{\rm OF}$ line is shown by the gray dotted line.

Table 3
Measured and Derived Host Galaxy and Outflow Properties

		J2310+1855	P183+05	P036+03
		119 μm Continuum		
$R_{1/2,119\ \mu m}$	[pc]	637 ± 53	1280 ± 45	707 ± 22
$S_{119\ \mu m}$	[mJy]	4.73 ± 0.0016	6.66 ± 0.0010	5.00 ± 0.0020
		OH 119 μm Emission (systemic)		
$S_{\rm OH\ 119\ \mu m}$	[Jy km s^{-1}]	⋯	0.28 ± 0.028	0.12 ± 0.022
$\sigma_{\rm Emis.}$	[km s^{-1}]	⋯	123 ± 13	45.9 ± 9.5
FWHM$_{\rm Emis}$	[km s^{-1}]	⋯	289 ± 31	108 ± 22
		OH 119 μm Absorption (outflow)		
$S_{\rm OH\ 119\ \mu m}$	[Jy km s^{-1}]	-0.42 ± 0.04	-0.19 ± 0.03	⋯
$N_{\rm OH\ 119\ \mu m}$	[10^{15} cm^{-2}]	8.90 ± 2.1	3.10 ± 0.059	⋯
EW$_{\rm OF}$	[km s^{-1}]	88.4 ± 21	28.9 ± 0.55	⋯
$\sigma_{\rm OF}$	[km s^{-1}]	140 ± 12	123 ± 19	⋯
FWHM$_{\rm OF}$	[km s^{-1}]	330 ± 29	290 ± 45	⋯
V_{50}	[km s^{-1}]	-334 ± 14	-534 ± 18	⋯
V_{84}	[km s^{-1}]	-473 ± 21	-656 ± 79	⋯
$V_{\rm max}$	[km s^{-1}]	-622 ± 85	-787 ± 222	⋯
$M_{\rm OF}$	[$10^8\ M_\odot$]	3.5–14	1.8–19	⋯
$\dot{M}_{\rm OF}$	[$M_\odot$ yr^{-1}]	190–760	75–800	⋯
$\dot{p}_{\rm OF}$	[10^{35} dyne]	4.0–16	2.5–26	⋯
$\dot{E}_{\rm OF}$	[10^{42} erg s^{-1}]	6.6–26	6.7–72	⋯
$\tau_{\rm OF}$	[Myr]	58–230	63–670	⋯
$\tau_{\rm OF+SFR}$	[Myr]	10–11	17–22	23

Note. Measured properties of the 119 μm dust continuum (size and flux), OH emission and absorption lines (with formal uncertainties from the fitting procedure), and derived properties of the molecular outflows.

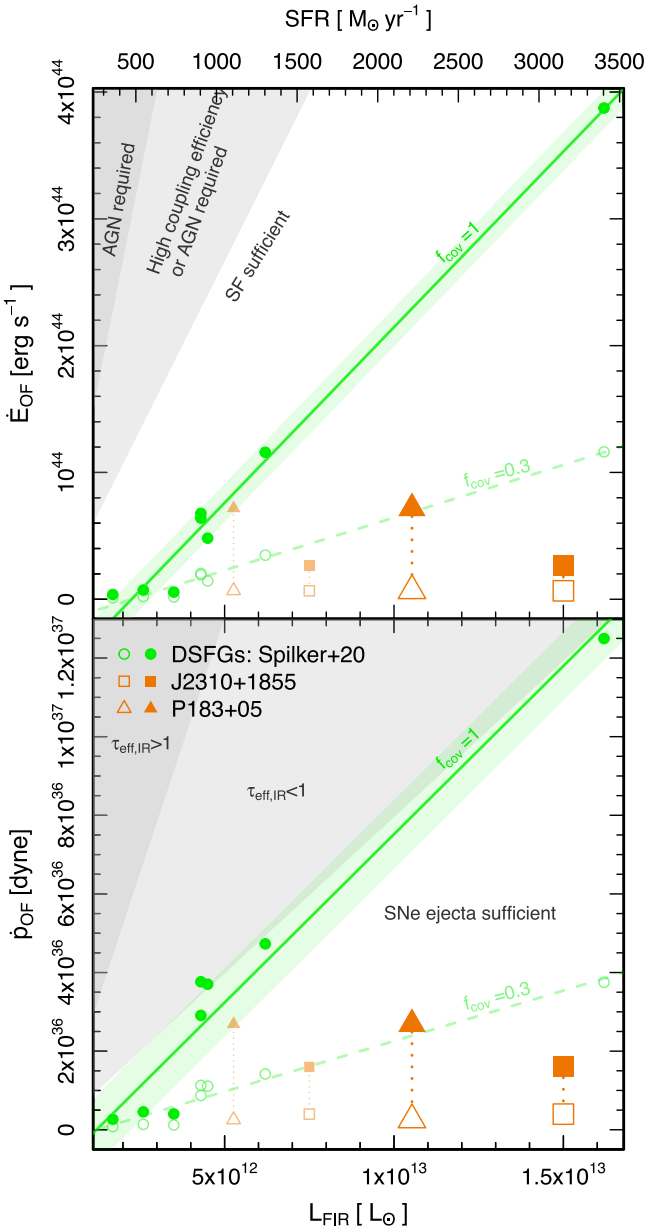

Figure 6. Energy (top) and momentum (bottom) flux as a function of $L_{\rm FIR}$ (bottom axis) and SFR (top axis) derived for the comparison sample of high-z DSFGs (Spilker et al. 2020a, 2020b) (green) and J2310+1855 and P183+05 (orange squares and triangles, respectively). Filled symbols indicate upper limits, assuming an outflow covering fraction of 1. Hollow symbols indicate lower limits for J2310+1855 and P183+05, assuming a covering fraction equal to the fractional OH absorption depth (25% and 9.4%, respectively), and values derived assuming an average covering fraction of 0.3 (González-Alfonso et al. 2017), for the DSFG sample. The smaller faint orange symbols indicate ranges for J2310+1855 and P183+05 assuming a 50% AGN contribution to $L_{\rm FIR}$ (see the main text). We indicate regions in the top panel where the energy injected via star formation, assuming a maximum coupling fraction to the interstellar medium of 40% (Sharma et al. 2014; Fielding et al. 2018), is equal to the energy flux of the outflow (white), where an unusually high coupling fraction or AGN contribution is required (light gray), and where an AGN is definitely required (darker gray). We indicate regions in the bottom panel where supernova ejecta provide sufficient momentum (white) and where radiation pressure on dust grains in an optically thin (light gray) or thick (darker gray) outflow is needed.

ORCID iDs

Kirsty M. Butler https://orcid.org/0000-0001-7387-0558
Matus Rybak https://orcid.org/0000-0002-1383-0746
Bram P. Venemans https://orcid.org/0000-0001-9024-8322
Fabian Walter https://orcid.org/0000-0003-4793-7880
Roberto Decarli https://orcid.org/0000-0002-2662-8803

References

Fielding, D., Quataert, E., & Martizzi, D. 2018, MNRAS, 481, 3325
González-Alfonso, E., Fischer, J., Spoon, H. W. W., et al. 2017, ApJ, 836, 11
Herrera-Camus, R., Sturm, E., Graciá-Carpio, J., et al. 2020, A&A, 633, L4
Sharma, P., Roy, A., Nath, B. B., & Shchekinov, Y. 2014, MNRAS, 443, 3463
Spilker, J. S., Aravena, M., Phadke, K. A., et al. 2020a, ApJ, 905, 86
Spilker, J. S., Phadke, K. A., Aravena, M., et al. 2020b, ApJ, 905, 85
Veilleux, S., Meléndez, M., Sturm, E., et al. 2013, ApJ, 776, 27